ACS APPLIED MATERIALS & INTERFACES

Research Article

www.acsami.org

High Performance and Stable N-Channel Organic Field-Effect Transistors by Patterned Solvent-Vapor Annealing

Dongyoon Khim,[‡] Kang-Jun Baeg,[§] Juhwan Kim,[‡] Minji Kang,[‡] Seung-Hoon Lee,[‡] Zhihua Chen,[∥] Antonio Facchetti,*[,∥] Dong-Yu Kim,*[,‡] and Yong-Young Noh*[,†]

[†]Department of Energy and Materials Engineering, Dongguk University, 26 Pil-dong, 3 ga, Jung-gu, Seoul 100-715, Republic of Korea

[‡]Heeger Center for Advanced Materials, School of Materials Science and Engineering, Department of Nanobio Materials and Electronics, Gwangju Institute of Science and Technology (GIST), 261 Cheomdan-gwagiro, Buk-gu, Gwangju 500-712, Republic of Korea

[§]Nano Carbon Materials Research Group, Korea Electrotechnology Research Institute (KERI), 12, Bulmosan-ro 10beon-gil, Seongsan-gu, Changwon, Gyeongsangnam-do 642-120, Republic of Korea

[∥]Polyera Corporation, 8045 Lamon Avenue, Skokie, Illinois 60077, United States

Supporting Information

ABSTRACT: We report the fabrication of high-performance, printed, *n*-channel organic field-effect transistors (OFETs) based on an *N*,*N*-dialkyl-substituted-(1,7&1,6)-dicyanoperylene-3,4:9,10-bis-(dicarboximide) derivative, PDI-RCN2, optimized by the solvent-vapor annealing (SVA) process. We performed a systematic study on the influence of solubility and the chemical structure of a solvent used for the SVA process on the ordering and orientation of PDI-RCN2 molecules in the thin film. The PDI-RCN2 film showed improved crystallinity under vapor annealing with the aliphatic 1,2-dichloro-ethane (DCE) as a marginal solvent. The *n*-type OFETs with DCE-vapor-annealed PDI-RCN2 show highly improved charge-carrier mobility of ∼0.5 $cm^2 V^{-1} s^{-1}$ and higher stability under gate bias stress than the pristine OFETs. This large performance improvement was mainly attributed to increased crystallinity of the semiconductor thin film, enhancing $\pi-\pi$ stacking. We also introduced a new method to pattern crystallinity of a certain region in the semiconducting film by selective exposure to the solvent vapor using a shadow mask. The crystal-patterned PDI-RCN2 OFETs exhibit decreased off-currents by ∼10× and improved gate bias stability by minimizing crosstalk, reducing leakage current between devices, and reducing the density of charge trap states of the organic semiconductor.

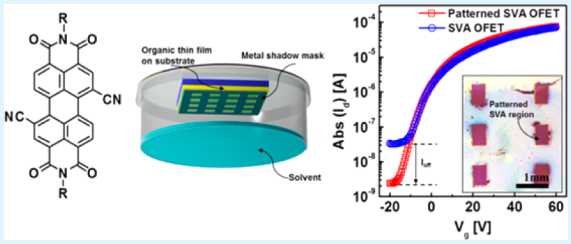

KEYWORDS: *organic field-effect transistors, solvent-vapor annealing, conjugated molecules, molecular orientation, bias stress, patterned crystallinity*

INTRODUCTION

In the past decade, a variety of innovative electronics and optoelectronics devices based on π-conjugated organic molecules have been developed.[1−3] Representative applications, such as organic light-emitting diode (OLED) displays, have been commercialized by a few pioneering companies, and new devices are on their way to the marketplace. This emerging technology could be progressed further by developing high-mobility, solution-processable, π-conjugated molecules and utilizing cost-effective, graphic-art printing methods for their main manufacturing process.[4−9] Recently, solution-processed small-molecule and polymeric semiconductors have demonstrated field-effect carrier mobilities exceeding 10 $cm^2 V^{-1} s^{-1}$, which are superior to amorphous-silicon semiconductors and comparable to those of solution-processed, amorphous metal-oxide or carbon-nanotube semiconductors.[10−12] Obviously, this unprecedented high mobility in organic semiconductors is a reminder that organic field-effect transistors (OFETs) may become suitable for a broad range of flexible electronic applications on plastic substrates such as microprocessors, flash memory, sensors, and backplane drivers for active-matrix flexible displays.[13−18] To achieve these high charge-carrier mobility with solution-processed conjugated molecules, the semiconductor film typically deposited on rigid Si−SiOx substrates and typically annealed at temperatures >100 °C for a relatively long time (>30 min) to improve the crystallinity, molecular ordering, and orientation, which are the most important parameters affecting OFET charge transport.[19,20] However, these substrates are impracticle for printed electronics, and equally important, this long thermal-annealing process is unsuitable for high-throughput, web-based, roll-to-roll printing processes, which are essential for low-cost flexible electronics.

Received: July 19, 2013
Accepted: October 18, 2013
Published: October 18, 2013

There have been a few approaches to improve the ordering of conjugated molecules without involving such a long and slightly high-temperature thermal-annealing process: (i) controlling the solvent evaporation rate during the thin-film deposition process using a high-boiling-point solvent and (ii) using solution aging, including additives, or both, to promote ordered aggregates such as crystalline nanowires or nanoparticles in solution.[21−23] One promising way to increase the molecular ordering and thin-film crystallinity in a relatively fast process at low temperature is exposing a preformed thin film to an environment filled with specific organic (or aqueous) solvent vapors, referred to as solvent-vapor annealing (SVA).[24] Penetration of the solvent vapor in the film of soluble π-conjugated molecules enables the formation of a "soft phase", which allows the molecules to reorganize with a higher degree of freedom than in a solid phase by decreasing the activation energy for rearrangement of the organic molecules.[24,25]

There have been several attempts to improve thin-film crystallinity and performance of OFETs by the SVA process.[26−30] The pioneering work by Loo and co-workers reported dramatically improved electrical properties of OFETs using *p*-type small molecules annealed under different solvent-vapor conditions.[26] They showed that the morphological/structural changes of the molecules due to SVA correlate with their OFET electrical performance, and the extent depended on the partitioning ability of the solvent vapor into the organic-semiconductor thin film. However, in contrast to extensive SVA research in the field of organic photovoltaics (OPVs), mainly with the purpose of morphological control of the donor−acceptor interface in an active layer film,[31,32] far fewer studies have been dedicated to show performance improvement for OFETs via the SVA process. Moreover, to the best of our knowledge, solvent annealing of organic semiconductors is mostly limited to *p*-type soluble acene-based materials.[26−28] Thus, there is still the need to better understand the exact mechanism during the SVA process as well as to broaden its applicability to *n*-type or ambipolar semiconductors for constructing complementary circuitries.

Here, we report a significant performance improvement for *n*-channel OFETs with a printable, *n*-channel, small-molecular organic semiconductor—an *N*,*N*-dialkyl-substituted-(1,7&1,6)-dicyanoperylene-3,4:9,10-bis(dicarboximide) derivative, PDI-RCN2—by using a rapid and simple SVA process. In this systematic study, a variety of solvents were selected and mainly classified by the solubility parameter of the perylene-diimide (PDI) derivative as: *good* [*p*-xylene, chlorobenzene (CB), 1,2-dichlorobenzene (DCB), and toluene], *marginal* [1,2-dichloroethane (DCE), acetone, 2-butanone, and 2-ethoxyetahanol (2E)], and *poor* [1-buthanol (1-BuOH)] solvents. Bottom-gated (BG) PDI-RCN2 OFETs showed the best OFET properties with electron mobilities as high as 0.5 $cm^2\ V^{-1}\ s^{-1}$ for films annealed for 10 min under DCE vapor, which is a marginal solvent with an aliphatic chemical structure. This large improvement over other aromatic solvents such as CB and *p*-xylene (~0.1 $cm^2\ V^{-1}\ s^{-1}$) mostly resulted from the formation of H-aggregates, leading to favorable $\pi-\pi$ stacking for efficient electron transport.

In addition, solvent-vapor-annealed OFETs show higher gate-bias stability compared to as-spun devices owing to the reduced density of trap states through improved ordering of the organic-semiconductor layer. Finally, we propose a new method to improve the crystallinity of specific regions of the semiconducting film by selective film exposure to the solvent vapor using a shadow mask. The crystal-patterned PDI-RCN2 film only at the channel regions of the OFET array, thus leaving the remaining area of the film with lower crystallinity or in the amorphous phase, decreases the off current by ~10×. More importantly, it also increases the gate-bias stability by minimizing crosstalk and the leakage current between devices and by reducing the density of charge trap states of the organic semiconductor.

EXPERIMENTAL SECTION

Spin-Coated OFET Device Fabrication. Bottom-gate/top-contact (BG/TC) OFETs were fabricated on a substrate, with a commercially available, heavily *n*-doped silicon Si(*n*++) wafer as the common gate electrode and thermally grown silicon dioxide (SiO_2, 300 nm thick) as the gate-dielectric layer, as shown in Figure 1a. After

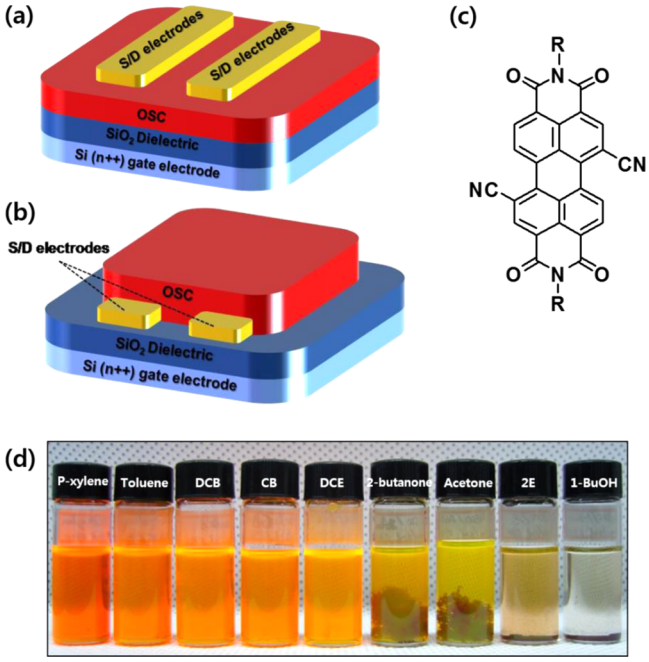

Figure 1. Schematic diagrams of the (a) bottom-gate/top-contact (BG/TC) (for spin-coated PDI-RCN2) and (b) bottom-gate/bottom-contact (BG/BC) (for inkjet-printed PDI-RCN2) OFET device structures. (c) Molecular structure of the *n*-channel small-molecular organic semiconductor, PDI-RCN2. (d) Digital camera image of the PDI-RCN2 solutions in different organic solvents with a concentration of 0.67 mg/mL.

cleaning the substrate in an ultrasonic bath using deionized water, acetone, and iso-propanol, respectively, for 10 min each, N_2 drying followed. ActivInk N1450 (Polyera Corp.), as the soluble, *n*-type small-molecular organic semiconductor PDI-RCN2, was purchased from Polyera Corp. and used without further purification. A PDI-RCN2 active layer was spin-coated on the as-cleaned SiO_2/Si(*n*++) substrate from a 10 mg/mL solution with chloroform and CB-mixed solvents in the mixing ratio 90:10 v/v%. The pristine PDI-RCN2 thin films were baked at 80 °C for 20 min on a hot plate in a N_2-filled glovebox and sequentially SVA-processed for different exposure durations (10 s to 20 min) in a covered Petri dish under each solvent-vapor condition. PDI-RCN2 thin film on substrate was held on with double-sided adhesive tape on the cover of the Petri dish. The solvent-vapor filling condition was created by releasing 50−200 μL of solvent in a Petri dish, heating it to 50−60 °C on a hot plate for 20 s to evaporate the solvents, and placing it in the same glovebox at room temperature for a desired amount of time. After the SVA process was complete, the thin films were baked at 80 °C again for ~30 min to completely remove any residual solvent. The OFET fabrication was

completed by evaporating Au (~50 nm thick) through a metal shadow mask to form the source/drain (S/D) electrodes on the PDI-RCN2 film, which had a channel length (L) and width (W) of 50 μm and 1.5 mm, respectively.

Inkjet-Printed OFET Device Fabrication. Inkjet-printed OFETs were fabricated with a bottom-gate/bottom-contact (BG/BC) device structure on a SiO_2 (300 nm thick)/Si(n++) substrate after cleaning, using the same sequence for spin-coated devices. The Au/Ni patterns (Au: S/D electrodes and Ni: adhesion layer) were fabricated using a conventional lift-off photolithography technique. The BC S/D patterns had L values of 2, 5, 10, and 20 μm and the same W value of 1.0 mm. The PDI-RCN2 solution (5 mg/mL concentration in CB) was inkjet-printed in air using a single-nozzle (piezoelectric type, Microfab Inc.) inkjet printer (Unijet, Korea) with an orifice diameter of 50 μm. The inkjet-printed organic semiconductor films were annealed at 80 °C for 20 min in a N_2-filled glovebox to remove the residual solvents. The SVA process was carried out using the same method for spin-coated transistors.

Characterization. The electrical current−voltage (I−V) characteristics of the OFETs were measured in a N_2-filled glovebox using a Keithley 4200 semiconductor characterization system. Surface morphology images were obtained using an atomic force microscope (AFM; Digital Instruments Multimode) controlled by a Nanoscope IIIa scanning probe microscope controller. X-ray diffraction (XRD) peaks were obtained using a Rigaku RINT 2000 diffractometer with Cu K_α radiation. The UV−Vis absorption spectrum was measured using a PerkinElmer Lambda 750 UV/vis spectrometer.

RESULTS AND DISCUSSION

Figures 1a and b show the configuration of bottom-gate/top-contact (BG/TC) and bottom-gate/bottom-contact (BG/BC) OFETs fabricated either by spin-coating or inkjet-printing the n-type organic semiconductor, PDI-RCN2. This material exhibits high electron field-effect mobility (μ_{FET}) with excellent air and bias stability and good solubility in common organic solvents.[33−36] Although it is reported that the excellent stability and solubility enabled high μ_{FET}'s of 1.0−1.5 $cm^2\ V^{-1}\ s^{-1}$ by spin-coating or inkjet-printing for top-gate/bottom-contact (TG/BC) OFETs,[37] the BG PDI-RCN2 OFETs with an as-spun thin film on an SiO_2 dielectric showed relatively poor device characteristics with a μ_{FET} value of ~0.02 $cm^2\ V^{-1}\ s^{-1}$ in our preliminary studies. Because most of the charge-carrier transport occurs within a few semiconductor molecular layers near the semiconductor−gate-dielectric interface in an OFET, molecular ordering and enhanced π−π stacking in the parallel direction of the dielectric surface as well as structural defects (grain boundaries) and impurities in the semiconductor layer are the most important parameters affecting OFET charge-transport characteristics.[38] Therefore, the poor performance of these bottom-gate OFETs based on the as-spun PDI-RCN2 films is not the result of the intrinsic electronic structure characteristic of this semiconductor but likely attributed to suboptimal surface morphology, large-sized aggregates, and a disconnected active-channel region, as can be seen in the optical-microscope image of Figure S1 in the Supporting Information. In general, by using a small-molecule solution, it is difficult to obtain a high-quality uniform thin film on a bare SiO_2 surface owing to the low viscosity and weak surface-adhesion energy of the small-molecule solution to the substrate, which typically leads to a limited selection of organic solvents and thus low-quality thin-film morphology.[39]

In this study, the SVA process was thus carried out by placing the samples in a specifically designed solvent-vapor-filled Petri dish after the deposition of the PDI-RCN2 thin film via spin-coating or inkjet-printing. The detailed SVA procedure is described in the Experimental Section. To take a close look at the relationship between the solvent and the resulting organic semiconductor morphology, we selected three classes of organic solvents based on the solubility of PDI-RCN2. Specifically: p-xylene, toluene, CB, and DCB are good solvents; DCE, 2-butanone, acetone, and 2E are marginal solvents; and 1-BuOH is a poor solvent. Figure 1d shows the distinctive solubility difference of PDI-RCN2 in various solvents. The fundamental parameters of the solvents used in this study, such as the solubility parameter and vapor pressure (i.e., boiling point), are listed in Table 1. The basic principle of solubility has been "like dissolves like". Although the solvents DCB and 2E have a similar solubility parameter value, ~10 $cal^{1/2}/cm^{3/2}$, more PDI-RCN2 molecules were dissolved in DCB, which is an aromatic solvent, compared to 2E, which is an aliphatic solvent (see Figure 1(d)) because the chemical structure of PDI-RCN2 consists of an aromatic core.[25,40]

Table 1. Fundamental Parameters of the Organic Solvents for Solvent-Vapor Annealing

solvent	solubility parameter[a] [$cal^{1/2}/cm^{3/2}$]	boiling point[a] [°C]	vapor pressure[b] at 20 °C [hPa]
p-xylene	8.85	138.3	15
toluene	8.91	110.6	29
1,2-dichlorobenzene	10	180	1.3
chlorobenzene	9.5	131.7	12
1,2-dichloroethane	9.76	83.5	79
2-butanone	9.3	80	105
acetone	9.77	56.0	240
2-ethoxyethanol	10	135	5
1-butanol	11.4	117.7	6.3

[a]Data compiled from ref 40. [b]Data compiled from ref 25.

Figure 2a shows the representative transfer characteristics of the pristine spin-coated PDI-RCN2 OFETs and solvent-vapor-annealed devices using DCB, DCE, and 1-BuOH for 10 min. The transfer characteristics of other solvent-vapor-annealed devices with p-xylene, toluene, CB, 2-butanone, acetone, and 2E are included in the Supporting Information (Figure S2). In addition, the basic parameters of all OFETs, including μ_{FET}, threshold voltage (V_{Th}), on/off current ratio (I_{on}/I_{off}), and subthreshold slope (SS), are summarized in Table 2. Through the SVA process, the overall device characteristics were improved compared to the pristine state, irrespective of the type of solvent. However, the degrees of improvement in μ_{FET}, I_{on}/I_{off}, and SS vary significantly with the solubility of PDI-RCN2 in the various (good, marginal, or poor) solvents, as can be seen from the solubility test results shown in Figure 1d. OFETs annealed with all good (p-xylene, toluene, DCB, and CB) and marginal (DCE, 2-butanone, acetone, and 2E) solvents showed high μ_{FET} of >0.1 $cm^2\ V^{-1}\ s^{-1}$. Notably, DCE-vapor-annealed transistors showed the maximum μ_{FET} of ~0.5 $cm^2\ V^{-1}\ s^{-1}$ (average μ_{FET} of ~0.3 $cm^2\ V^{-1}\ s^{-1}$) in the saturation region at a drain voltage (V_d) of +60 V, which is >20 times higher than the average μ_{FET} of 0.01−0.02 $cm^2\ V^{-1}\ s^{-1}$ for the as-spun devices. On the other hand, when annealing with the poor solvent 1-BuOH, the devices showed an only slightly improved μ_{FET} of ~0.064 $cm^2\ V^{-1}\ s^{-1}$ (approximately 3-fold increase).

In addition, also the inkjet-printed BG/BC PDI-RCN2 OFETs exhibited significantly improved device characteristics

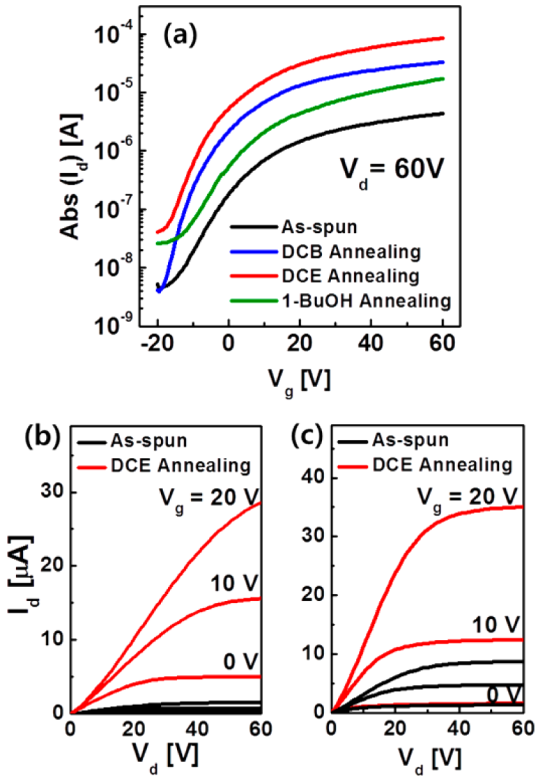

Figure 2. (a) Transfer characteristics (I_d vs V_g) of the spin-coated BG/TC PDI-RCN2 OFETs: as-spun thin film and those after solvent-vapor annealing with DCB, DCE, and 1-BuOH. Output characteristics (I_d vs V_d) of the (b) spin-coated BG/TC PDI-RCN2 OFETs and (c) inkjet-printed BG/BC PDI-RCN2 OFETs with the as-spun thin film and after SVA with DCE.

after the SVA process. As shown in Figure S3 in the Supporting Information, pristine, inkjet-printed PDI-RCN2 OFETs from CB exhibited slightly higher μ_{FET} (0.05 $cm^2\ V^{-1}\ s^{-1}$) than that of spin-coated devices presumably owing to improved film crystallinity resulting from the slow evaporation of the solvent during the inkjet printing process, improved contact resistance, or both, as shown in the linear region of the output plots (I_d vs V_d) in Figures 2b and 2c.[36]

After the SVA process, μ_{FET} of inkjet-printed devices also increased to the maximum values of ~0.41 $cm^2\ V^{-1}\ s^{-1}$ (average μ_{FET} of ~0.38 $cm^2\ V^{-1}\ s^{-1}$) and ~0.31 $cm^2\ V^{-1}\ s^{-1}$ (average μ_{FET} of ~0.27 $cm^2\ V^{-1}\ s^{-1}$) using DCE (marginal) and DCB (good) solvent vapors, respectively, whereas, 1-BuOH solvent vapor (poor) had no significant effect on the OFET performance.

To investigate the origin of the significant OFET performance improvement through the SVA process, we implemented morphological and structural studies to PDI-RCN2 by selecting three distinctive organic solvents as the good (DCB), marginal (DCE), and poor (1-BuOH) solvents. From PDI-RCN2 solubility tests, the estimated solubility in DCB and DCE is ~12.5 and ~2.5 mg/mL, respectively. The solubility in 1-BuOH is too low to be measured accurately. Figures 3a–d show the tapping-mode AFM images of the as-spun PDI-RCN2 film (Figure 3a), and films that were solvent-vapor-annealed with DCB (Figure 3b), DCE (Figure 3c), and 1-BuOH (Figure 3d). In the pristine film, large-sized aggregates and very rough top-surface topology were observed, with a root-mean-square roughness (R_q) above 90 nm (10 μm × 10 μm) without evidence of crystalline features (Figure 3a). Moreover, XRD measurements carried out on the corresponding as-spun PDI-RCN2 thin film also showed a weak reflection at 2θ = 4.8°, corresponding 18.4 Å to the (001) plane without multiorder peaks, as shown in Figure 3e. In contrast, the film morphology changed remarkably after the SVA process even for a short exposure duration (10 min). Interestingly, the solvent-vapor-annealed film using marginal DCE solvent showed dramatic structural changes going from aggregated heaps to crystalline nanoribbons, as can be seen in Figure 3c. The intensity of the XRD peak at 2θ = 4.8° increased remarkably by >5× after SVA with DCE, compared to the pristine film, with the appearance of multiorder reflections located at 2θ = 9.6° and 14.4° (inset of Figure 3e). In a previous report, the vapor-deposited PDI molecule showed similar X-ray patterns with 17.9 Å to the (001) plane, where tilt angles relative to the substrate normal of 55° were estimated, which is favorable molecular orientation for charge transport.[41] In contrast, the other solvent vapors, DCB and 1-BuOH, did not significantly alter the rough morphology. The surface roughness of the films was slightly reduced to R_q =

Table 2. Fundamental Parameters of PDI-RCN2 OFETs after the SVA Process[a]

solvent	process	μ_{FET} [$cm^2\ V^{-1}\ s^{-1}$]	V_{Th} [V]	I_{on}/I_{off}	SS [V/dec.]
pristine	spin-coating[b]	0.015 (±0.05)	−10 to −21	~10^3	10
	inkjet-printing[c]	0.050 (±0.01)	−16 to −8	~10^3	9–10
p-xylene	spin-coating	0.11 (±0.02)	−4 to −17	~10^4	6–7
	inkjet-printing	0.28 (±0.05)	−5 to −8	~5×10^4	6–8
toluene	spin-coating	0.10 (±0.03)	−2 to −19	~10^4	7–8
DCB	spin-coating	0.12 (±0.01)	−4 to −15	~10^4	4–5
	inkjet-printing	0.27 (±0.04)	−4 to −6	~10^4	6–8
CB	spin-coating	0.11 (±0.02)	−6 to −17	~10^4	5–6
DCE	spin-coating	0.30 (±0.04)	−9 to −17	~5×10^3	5–6
	inkjet-printing	0.38 (±0.03)	−11 to −8	~10^4	6–7
2-butanone	spin-coating	0.14 (±0.02)	−1 to 5	~5×10^4	4–5
acetone	spin-coating	0.13 (±0.03)	−10 to −18	~10^4	4–5
2-ethoxyethanol	spin-coating	0.10 (±0.02)	−14 to −20	~5×10^3	7–8
1-butanol	spin-coating	0.064 (±0.01)	−9 to −13	~10^3	7–8
	inkjet-printing	0.050 (±0.02)	−10 to 0	~10^4	10–12

[a]Electrical parameters were calculated at the saturation region (V_d = 60 V) using gradual channel approximation equations. [b]Spin-coated OFETs (BG/TC). [c]Inkjet-printed OFETs (BG/BC).

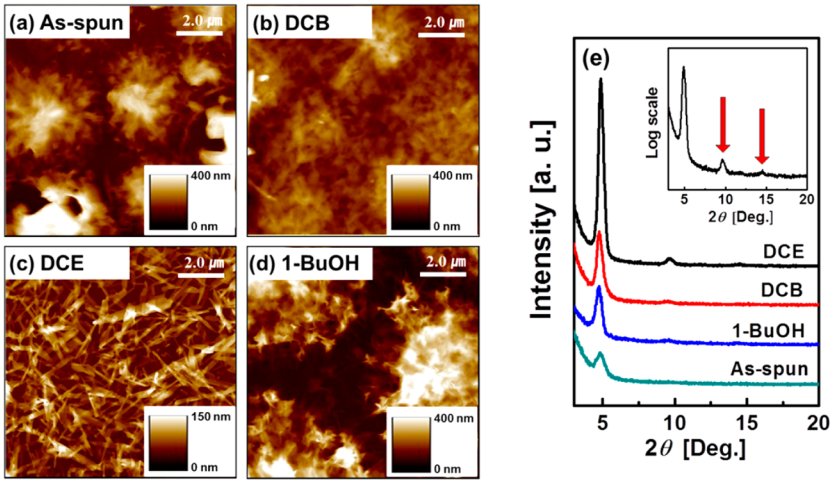

Figure 3. AFM images of the (a) as-spun PDI-RCN2 thin film on a SiO_2 substrate and those after the SVA process with (b) DCB, (c) DCE, and (d) 1-BuOH for 10 min. (e) Out-of-plane X-ray diffraction patterns of the PDI-RCN2 thin film on a SiO_2 substrate (as-spun; DCB-, DCE-, and 1-BuOH-annealed for 10 min). The inset shows a logarithmic-scale plot of the DCE annealed film, indicating multiorder peaks at $2\theta = 9.6°$ and 14.4°.

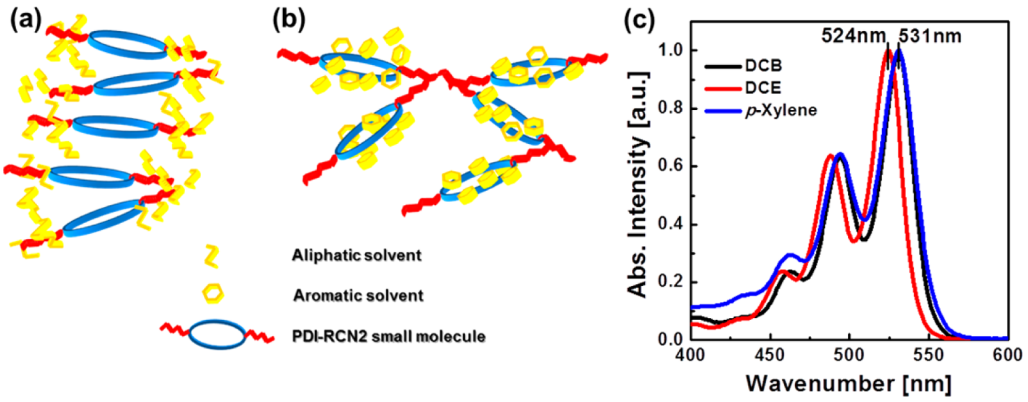

Figure 4. Schematic diagram of (a) ordered molecular packing induced by an aliphatic solvent vapor such as DCE and (b) less ordered molecular packing induced by an aromatic solvent vapor such as DCB and *p*-xylene. (c) UV−Vis absorption spectra of PDI-RCN2 solutions in several solvents (DCB and *p*-xylene as aromatic solvents; DCE as an aliphatic solvent).

~40 nm and ~70 nm after the SVA process with DCB and 1-BuOH, respectively (Figures 3b and d). These results are consistent with the slightly enhanced intensity of XRD peaks compared to that of the pristine film. The poor solvent 1-BuOH did not cause any significant morphological changes since unsolvated small molecules cannot reorganize easily. These solvents were thus ineffective to optimize film morphology at the OFET semiconductor−dielectric interface presumably because of significant dewetting (DCB) and inefficient recrystallization (1-BuOH).[26] We could therefore conclude that the marginal solvent (DCE) vapors enable the formation of more uniform and highly crystalline organic thin-film structures. The improved crystallinity of the DCE-vapor-annealed PDI-RCN2 films can be presumably explained by different solubility of aromatic cores and aliphatic side chains to solvents used for SVA processes. Typical soluble conjugated molecules consist of a rigid aromatic core (e.g., cyanated perylene in PDI-RCN2) and flexible, solubilizing side groups (e.g., alkyl chain in PDI-RCN2). The aromatic core and aliphatic side chains show different solubility in aromatic and aliphatic solvents.

As illustrated in Figure 4a,b, aliphatic organic solvents such as DCE and acetone predominately dissolve the side alkyl chains of PDI-RCN2 instead of the aromatic core. The relatively less solvated aromatic cores allow intermolecular $\pi-\pi$ overlap with each other, leading to molecules stacked in a plane-to-plane configuration, which can provide good charge transport properties. On the other hand, aromatic organic solvents such as toluene, *p*-xylene, CB, and DCB could mostly solvate the aromatic core rather than the alkyl side chains of PDI-RCN2. Therefore, relatively less-solvated alkyl side chains can easily aggregate each other through van der Waals interaction leading to randomly ordered molecular conformation. Figure 4c shows UV−Vis absorption spectra of PDI-RCN2 solutions in aliphatic (DCE) or aromatic (DCB and *p*-xylene) solvents. The maximum absorption peak of the DCE solution is located at λ_{max} = 524 nm which is clearly blue-shifted by ~7 nm from that of the DCB or *p*-xylene solution (λ_{max} = 531 nm). This result indicates more intense face-to-face stacked aromatic rings in DCE solution compared to those in DCB and *p*-xylene solution.[42,43] Therefore, the PDI-RCN2 molecules in the DCE solvent led to a tendency of more ordered rearrangement between the molecules.

Figure 5 shows μ_{FET} of the PDI-RCN2 OFETs as a function of the solvent vapor exposure time. At the initial stage (within 5 min) of the SVA process, μ_{FET} increases nearly at the same rate, which means that the solvent vapors evaporated quickly at the initial stage with similar rates and completely filled the closed

dx.doi.org/10.1021/am4029075 | ACS Appl. Mater. Interfaces 2013, 5, 10745−10752

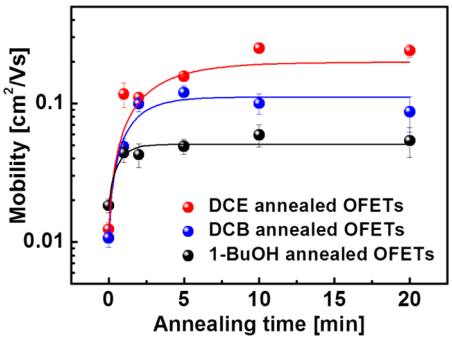

Figure 5. μ_{FET} of PDI-RCN2 OFETs as a function of DCE, DCB, and 1-BuOH solvent-vapor-annealing time.

jar at a substrate temperature of 50−60 °C, followed by penetration into the organic semiconductor films and changing the film structures. Once the closed jar was filled with solvent vapor, its capability to affect the semiconductor film morphology is critically determined by the semiconductor solubility and the chemical structure of the solvent used. Therefore, OFETs annealed with 1-BuOH were the first to reach the optimal performance limits for this solvent (~0.05 $cm^2\ V^{-1}\ s^{-1}$) without further improvement with time, followed by the DCB-annealed devices (~0.1 $cm^2\ V^{-1}\ s^{-1}$). The DCE-annealed devices exhibited the highest electron mobility of ~0.3 $cm^2\ V^{-1}\ s^{-1}$. Regardless of the type of solvent, the μ_{FET} value of all SVA-processed OFETs rapidly increased within the first 1−2 min of exposure. This means that the PDI-RCN2 film ordering and crystallinity developed very quickly with the help of DCE vapors. After further optimization of the SVA process by controlling several experimental parameters such as solvent solubility, polarity, and vapor pressure as well as annealing temperature and time, the processing time could be remarkably reduced to even less than 1−2 min. SVA thus enables the formation of a high-quality thin-film structure with fast processing time as compared to typical thermal-annealing processes requiring high temperature and relatively long durations of at least 10 min. In this regard, the SVA process can be a promising method with high compatibility and high throughput in continuous printing-based roll-to-roll processes for fabrication of soft electronic devices.

To further verify SVA's effects on operational stability and reliability of PDI-RCN2 OFETs, several FET electrical parameters were evaluated on bias-stress tests for both as-spun and DCE-vapor-annealed devices. Assuming that the electron mobility is constant in the saturation region, the evolution of the V_{Th} shift is extracted from the change in the drain current $I_d(t)$ by eq 1 as follows

$$|\Delta V_{Th}|(t) = \left(1 - \sqrt{\frac{I_d(t)}{I_0}}\right)|V_g - V_{Th,0}| \quad (1)$$

where $I_d(t)$ is the drain current as a function of time t; V_g is the applied gate bias; and $V_{Th,0}$ and I_0 are the initial threshold voltage and drain current, respectively. Figures 6a and b show normalized I_d decay and the corresponding V_{Th} shift in the PDI-RCN2 OFETs with a pristine film and after DCE-SVA under constant bias conditions at V_g = +60 V and V_d = +60 V for 2000 s. It shows that the normalized I_d of DCE-SVA OFETs decayed by ~46% from its initial value, which was ~11% less than that of the as-spun device with decaying of ~57% under the same bias-stress conditions. This result indicated that mobile charge-carrier trapping was remarkably reduced after the SVA process with an aliphatic marginal solvent. The trapped charge (Q_t) screened the gate electric field, which in turn caused a shift in V_{Th} as follows: $Q_t = C_i \times \Delta V_{Th}$, where C_i is the gate dielectric capacitance. Therefore, ΔV_{Th} in Figure 6b followed the same trend as I_d decay, which resulted in a reduced positive V_{Th} shift for the DCE-solvent-vapor-annealed OFET device (shifted by ~13.5 V) compared to the as-spun device (shifted by ~16.3 V) after 2000 s. For OFETs, trapping of mobile-charge carriers typically takes place in a bulk semiconductor film mostly at the grain boundaries or in noncrystalline phases between the organic-semiconductor crystals via the formation of bipolarons or at the semiconductor−dielectric interfaces.[44−47]

Obviously, we verified that the PDI-RCN2 thin film was converted to a highly crystalline phase and large-sized microribbons after exposure to the DCE solvent vapor. Thus, the reduced number density of trap states led to improved bias stability for the SVA-processed OFET devices. We also calculated the number of interface traps (N_{it}) using the subthreshold slope (SS) values from the $I-V$ transfer characteristics. When the densities of deep bulk states and interface states are independent of energy, N_{it} can be estimated by eq 2 as follows

$$N_{it} = \left[\frac{SS \cdot \log(e)}{kT/q} - 1\right]\frac{C_i}{q} \quad (2)$$

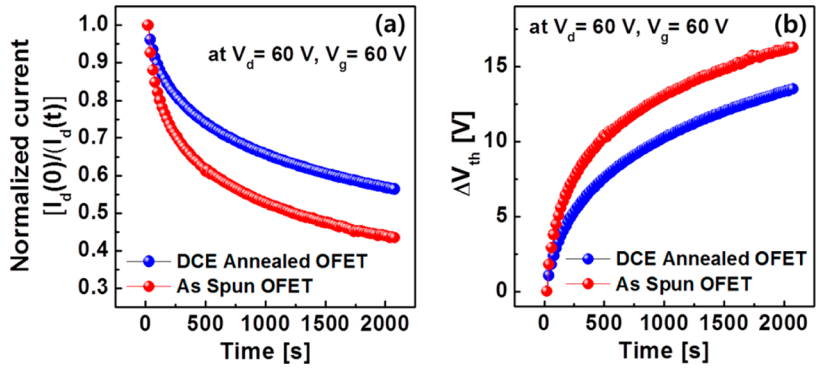

Figure 6. Bias stress measurement on as-spun and DCE-annealed PDI-RCN2 OFETs. (a) Normalized current under constant bias stress (at V_d = 60 V and V_g = 60 V). (b) Shift of threshold voltage as a function of time under the same conditions.

where C_i is the gate dielectric capacitance, q the electronic charge, k the Boltzmann constant, and T the absolute temperature. The estimated N_{it} of the PDI-RCN2 OFET was significantly reduced to 5.1×10^{12} cm^{-2} after SVA with DCE compared to the value of 1.03×10^{13} cm^{-2} for pristine PDI-RCN2 devices.

As shown in Figure 2a, the DCE solvent vapor-annealed OFETs exhibited high saturation current up to ~0.1 mA at V_d = +60 V and V_g = +60 V, while the off-current was also appreciably increased by more than 1 order of magnitude (>30 nA) compared to the leakage current of the as-spun devices. It was mainly attributed to the higher leakage current between devices owing to increased film crystallinity upon SVA treatment. The high off-current has to be reduced as much as possible because it leads to high power dissipation in the off states of microprocessors or display drivers.[13] To substantially decrease the high off-state current in solvent-vapor-annealed OFET devices, we propose a new method to pattern crystallinity in specific regions for a continuous semiconducting film. This method consists of exposing selected semiconductor areas to solvent vapor using a shadow mask. Figure 7a shows a schematic diagram of the procedure, and an optical microscope image of the corresponding SVA-patterned PDI-RCN2 film is shown in the inset of Figure 7b. As can be seen in Figure 7b, SVA-patterned PDI-RCN2 OFETs exhibited lower off-state leakage current by more than 1 order of magnitude than the unpatterned devices, while the on-state saturation current and charge-carrier mobilities were almost identical at ~0.21 and ~0.17 cm^2 V^{-1} s^{-1} for both patterned and unpatterned OFETs, respectively. The reduction in the off-state current resulted from the reduced crystallinity of the regions between the patterned (channel) areas. This result is consistent with previous reports where the off-current can be decreased by patterning the organic-semiconductor film.[13,48] In particular, the off-current of ~2 nA in the patterned PDI-RCN2 OFETs was almost similar to that of as-spun PDI-RCN2 OFET devices. Therefore, shadow-mask patterning during the SVA process enabled the fabrication of high-performance OFETs with excellent bias-stress stabilities by offering improved crystallinity of the semiconducting film and simultaneously low off-state current by minimizing the parasitic leakage current between devices.

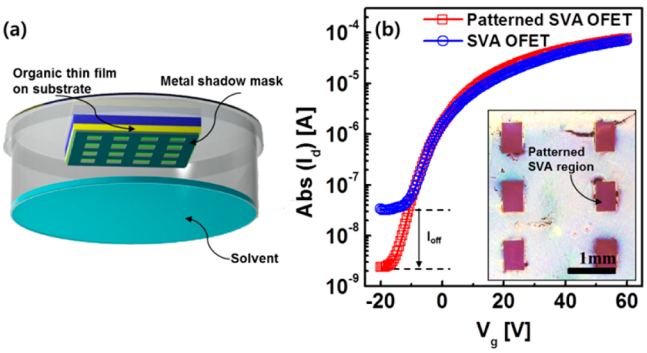

Figure 7. (a) Schematic diagram of the patterned solvent-vapor-annealing process using a metal shadow mask. (b) Transfer characteristics of SVA and patterned SVA PDI-RCN2 OFETs. The inset shows an optical microscope image of a patterned, crystallized PDI-RCN2 thin film that was exposed to solvent vapor with a shadow mask.

CONCLUSIONS

In conclusion, the fabrication of high-performance, solution-processed, *n*-type PDI-RCN2 OFETs by the solvent-vapor-annealing process was demonstrated. Through short exposure to a specific solvent vapor, the morphology and crystallinity of the film were dramatically improved. DCE-vapor-annealed OFET devices showed the highest electron mobility up to 0.5 cm^2 V^{-1} s^{-1} and an average mobility of ~0.3 cm^2 V^{-1} s^{-1}, which was 10−20 times higher than the values for as-spun pristine thin-film devices before SVA. The significant performance improvement with a marginal solvent exposure correlates with the solubility parameter of PDI-RCN2 with DCE. Thus, marginal organic solvents such as DCE partially swell the semiconductor film into the pseudoliquid phase, thereby favoring molecular rearrangement and reorganization of the semiconductor molecules during SVA. In addition, the DCE-vapor-annealed OFET device showed high reliability under constant bias-stress conditions compared to the as-spun device owing to the reduced density state density. Finally, we demonstrated a new method to improve the crystallinity of specific semiconductor regions by selective vapor solvent exposure using a shadow mask. The shadow-mask-patterned SVA OFETs exhibited high on-state saturation current and low off-state leakage current (high I_{on}/I_{off} ratio up to ~10^5). This SVA process provides a simple route in a very short process time (~1−2 min) to obtain highly crystalline thin films enabling high charge-carrier mobility, stable bias, and operational stability *n*-channel FETs. We also believe that this process is also compatible with high-throughput roll-to-roll fabrication of printed soft electronics.

ASSOCIATED CONTENT

Supporting Information

Optical microscope image of a spin-coated PDI-RCN2 thin film and transfer characteristics of solvent-annealed OFETs (spin-coated OFETs with *p*-xylene, toluene, CB, 2-butanone, acetone, and 2-ethoxyethanol and inkjet-printed OFETs with DCE, *p*-xylene, DCB, and 1-BuOH SVA process). This material is available free of charge via the Internet at http://pubs.acs.org.

AUTHOR INFORMATION

Corresponding Authors

*E-mail: afacchetti@polyera.com.
*E-mail: kimdy@gist.ac.kr.
*E-mail: yynoh@dongguk.edu.

Notes

The authors declare no competing financial interest.

ACKNOWLEDGMENTS

This work was supported by the National Research Foundation of Korea (NRF) grant funded by the Korea government (MSIP) (No. 2013-059210) and a grant from the Centre for Advanced Soft Electronics under the Global Frontier Research Program of MEST, Korea (code no. 2013-073183), and was supported by the Dongguk University Research Fund of 2013.

REFERENCES

(1) Sirringhaus, H. *Adv. Mater.* **2005**, *17*, 2411−2425.
(2) Facchetti, A. *Chem. Mater.* **2011**, *23*, 733−758.
(3) Farchioni, R.; Grosso, G. *Organic Electronic Materials: Conjugated Polymers and Low Molecular Weight Organic Solids*; Springer: Berlin, 2001.

(4) Sirrinhaus, H.; Kawase, T.; Friend, R. H.; Shimoda, T.; Inbasekaran, M.; Wu, W.; Woo, E. P. *Science* **2000**, *290*, 2123−2126.
(5) Noh, Y.-Y.; Zhao, N.; Caironi, M.; Sirringhaus, H. *Nat. Nanotechnol.* **2007**, *2*, 784−789.
(6) Krebs, F. C.; Fyenbo, J.; Jorgensen, M. *J. Mater. Chem.* **2010**, *20*, 8994−9001.
(7) Baeg, K.-J.; Khim, D.; Kim, D.-Y.; Jung, S.-W.; Koo, J. B.; You, I.-K.; Yan, H.; Facchetti, A.; Noh, Y.-Y. *J. Polym. Sci., Part B: Polym. Phys.* **2011**, *49*, 62−67.
(8) Giri, G.; Verploegen, E.; Mannsfeld, S. C. B.; Atahan-Evrenk, S.; Kim, D. H.; Lee, S. Y.; Becerril, H. A.; Aspuru-Guzik, A.; Toney, M. F.; Bao, Z. *Nature* **2011**, *480*, 504−508.
(9) Khim, D.; Han, H.; Baeg, K.-J.; Kim, J.; Kwak, S.-W.; Kim, D.-Y.; Noh, Y.-Y. *Adv. Mater.* **2013**, *25*, 4302−4308.
(10) Li, J.; Zhao, Y.; Tan, H. S.; Guo, Y.; Di, C.-A.; Yu, G.; Liu, Y.; Lin, M.; Lim, S. H.; Zhou, Y.; Su, H.; Ong, B. S. *Sci. Rep.* **2012**, *2*, 754.
(11) Smith, J.; Zhang, W.; Sougrat, R.; Zhao, K.; Li, R.; Cha, D.; Amassian, A.; Heeney, M.; McCulloch, I.; Anthopoulos, T. D. *Adv. Mater.* **2012**, *24*, 2441−2446.
(12) Minemawari, H.; Yamada, T.; Matsui, H.; Tsutsumi, J.; Haas, S.; Chiba, R.; Kumai, R.; Hasegawa, T. *Nature* **2011**, *475*, 364−367.
(13) Gelinck, G. H.; Huitema, H. E. A.; Van Veenendaal, E.; Cantatore, E.; Schrijnemakers, L.; Van der Putten, J.; Geuns, T. C. T.; Beenhakkers, M.; Giesbers, J. B.; Huisman, B. H.; Meijer, E. J.; Benito, E. M.; Touwslager, F. J.; Marsman, A. W.; Van Rens, B. J. E.; de Leeuw, D. M. *Nat. Mater.* **2004**, *3*, 106−110.
(14) Klauk, H.; Zschieschang, U.; Pflaum, J.; Halik, M. *Nature* **2007**, *445*, 745−748.
(15) Gelinck, G.; Heremans, P.; Nomoto, K.; Anthopoulos, T. D. *Adv. Mater.* **2010**, *22*, 3778−3798.
(16) Baeg, K.-J.; Caironi, M.; Noh, Y.-Y. *Adv. Mater.* **2013**, *25*, 4210−4244.
(17) Scott, J. C.; Bozano, L. D. *Adv. Mater.* **2007**, *19*, 1452−1463.
(18) Heremans, P.; Gelinck, G. H.; Muller, R.; Baeg, K.-J.; Kim, D.-Y.; Noh, Y.-Y. *Chem. Mater.* **2011**, *23*, 341−358.
(19) Mas-Torrent, M.; Rovira, C. *Chem. Rev.* **2011**, *111*, 4833−4856.
(20) Kline, R. J.; McGehee, M. D.; Kadnikova, E. N.; Liu, J.; Frechet, J. M. J. *Adv. Mater.* **2003**, *15*, 1519−1522.
(21) Yang, H.; Shin, T. J.; Yang, L.; Cho, K.; Ryu, C. Y.; Bao, Z. *Adv. Funct. Mater.* **2005**, *15*, 671−676.
(22) Ong, B. S.; Wu, Y.; Liu, P.; Gardner, S. *Adv. Mater.* **2005**, *17*, 1141−1144.
(23) Park, Y. D.; Lee, H. S.; Choi, Y. J.; Kwak, D.; Cho, J. H.; Lee, S.; Cho, K. *Adv. Funct. Mater.* **2009**, *19*, 1200−1206.
(24) De Luca, G.; Treossi, E.; Liscio, A.; Mativetsky, J. M.; Monsù Scolaro, L.; Palermo, V.; Samorì, P. *J. Mater. Chem.* **2010**, *20*, 2493−2498.
(25) Reichardt, C.; Welton, T. *Solvents and Solvent Effects in Organic Chemistry*; Wiley-VCH: Weinheim, 2011.
(26) Dickey, K. C.; Anthony, J. E.; Loo, Y.-L. *Adv. Mater.* **2006**, *18*, 1721−1726.
(27) Lee, S. S.; Kim, C. S.; Gomez, E. D.; Purushothuman, B.; Toney, M. F.; Wang, C.; Hexemer, A.; Anthony, J. E.; Loo, Y.-L. *Adv. Mater.* **2009**, *21*, 3605−3607.
(28) Lee, W. H.; Kim, D. H.; Cho, J. H.; Jang, Y.; Lim, J. A.; Kwak, D.; Cho, K. *Appl. Phys. Lett.* **2007**, *91*, 092105.
(29) Liu, C.; Minari, T.; Lu, X.; Kumatani, A.; Takimiya, K.; Tsukagoshi, K. *Adv. Mater.* **2011**, *23*, 523−526.
(30) Liu, Y.; Shi, Q.; Dong, H.; Tan, J.; Hu, W.; Zhan, X. *Org. Electron.* **2012**, *13*, 2372−2378.
(31) Li, G.; Yao, Y.; Yang, H.; Shrotriya, V.; Yang, G.; Yang, Y. *Adv. Funct. Mater.* **2007**, *17*, 1636−1644.
(32) Jo, J.; Kim, S.-S.; Na, S.-I.; Yu, B.-K.; Kim, D.-Y. *Adv. Funct. Mater.* **2009**, *19*, 866−874.
(33) Würthner, F.; Stolte, M. *Chem. Commun.* **2011**, *47*, 5109−5115.
(34) Ng, T. N.; Sambandan, S.; Lujan, R.; Arias, A. C.; Newman, C. R.; Yan, H.; Facchetti, A. *Appl. Phys. Lett.* **2009**, *94*, 233307.
(35) Baeg, K.-J.; Khim, D.; Kim, J.; Kang, M.; You, I.-K.; Kim, D.-Y.; Noh, Y.-Y. *Org. Electron.* **2011**, *12*, 634−640.
(36) Khim, D.; Baeg, K.-J.; Yu, B.-K.; Kang, S.-J.; Kang, M.; Chen, Z.; Facchetti, A.; Kim, D.-Y.; Noh, Y.-Y. *J. Mater. Chem. C* **2013**, *1*, 1500−1506.
(37) Polyera Home Page. http://www.polyera.com (accessed Oct 14, 2013).
(38) Sirringhaus, H. *Adv. Mater.* **2005**, *17*, 2411−2425.
(39) Allard, S.; Forster, M.; Souharce, B.; Thiem, H.; Scherf, U. *Angew. Chem., Int. Ed.* **2008**, *47*, 4070−4097.
(40) *Handbook of Organic Solvent*; Lide, D. R., Ed.; CRC Press: Boca Raton, 1995.
(41) Jones, B. A.; Ahrens, M. J.; Yoon, M. H.; Facchetti, A.; Marks, T. J.; Wasielewski, M. R. *Angew. Chem., Int. Ed.* **2004**, *43*, 6363−6366.
(42) Cornil, J.; Beljonne, D.; Calbert, J. P.; Bredas, J. L. *Adv. Mater.* **2001**, *13*, 1053−1067.
(43) Lewis, F. D.; Wu, T.; Burch, E. L.; Bassani, D. M.; Yang, J. S.; Schneider, S.; Jager, W.; Letsinger, R. L. *J. Am. Chem. Soc.* **1995**, *117*, 8785−8792.
(44) Sharma, A.; Mathijssen, S. G. J.; Smits, E. C. P.; Kemerink, M.; de Leeuw, D. M.; Bobbert, P. A. *Phys. Rev. B* **2010**, *82*, 075322.
(45) Street, R. A.; Salleo, A.; Chabinyc, M. L. *Phys. Rev. B* **2003**, *68*, 085316.
(46) Tello, M.; Chiesa, M.; Duffy, C. M.; Sirringhaus, H. *Adv. Funct. Mater.* **2008**, *18*, 3907−3913.
(47) Sirringhaus, H. *Adv. Mater.* **2009**, *21*, 3859−3873.
(48) Baeg, K.-J.; Khim, D.; Kim, D.-Y.; Koo, J. B.; You, I.-K.; Choi, W. S.; Noh, Y.-Y. *Thin Solid Films* **2010**, *518*, 4024−4029.